Journal of Zhejiang University-SCIENCE B (Biomedicine & Biotechnology) in press
www.jzus.zju.edu.cn; www.springer.com/journal/11585
E-mail: jzus_b@zju.edu.cn

https://doi.org/10.1631/jzus.B23Z0003

Cellulose nanofibril matrix drives the dynamic formation of spheroids

Yi LU[1,2,3*], Guo LI[1,2*], Yeqiu LI[2], Yuan YAO[1,2,3]✉

[1]*College of Chemical and Biological Engineering, Zhejiang University, Hangzhou, Zhejiang, 310027, China*
[2]*ZJU-Hangzhou Global Scientific and Technological Innovation Center, Zhejiang University, Hangzhou 311215, China*
[3]*School of Physical Science and Technology, ShanghaiTech University, 393 Middle Huaxia Road, Shanghai, 201210 China*

Abstract: Multicellular spheroids, which mimic the natural organ counterparts, allow the prospect of drug screening and regenerative medicine. However, their application is hampered by low processing efficiency or limited scale. This study introduces an efficient method to drive rapid multicellular spheroid formation by a cellulose nanofibril matrix. This matrix enables the facilitated growth of spheroids (within 48 hours) through multiple cell assembly into size-controllable aggregates with well-organized physiological microstructure. The efficiency, dimension, and conformation of the as-formed spheroids depend on the concentration of extracellular nanofibrils, the number of assembled cells, and the heterogeneity of cell types. The above strategy allows the robust formation mechanism of compacted tumoroids and hepatocyte spheroids.

Key words: Cellulose; Nanofibril; Matrix; Self-Assembly; Spheroid

Introduction

The assembly of spatially ordered multiple cells as spheroids or tumoroids is a promising avenue for tissue engineering and personalized medicine (Tuveson and Clevers, 2019; Gonzalez-Rodriguez et al., 2012; Steinberg, 1962; Tevis et al., 2017; Chen et al., 2023). Researchers require models to replicate the multicellular nature and 3D stromal environment in an in vivo tumor (Tevis et al., 2017). Biomacromolecules from the extracellular matrix (ECM) are critical to connect the material surfaces and living tissues. These ECM biomacromolecules with specific topology as nanofibril or network between the material-organism interface are essential for organogenesis (Ren et al., 2019) and play a significant role in remodeling the surrounding tumor microenvironment (Huang et al., 2015; Yeatts et al., 2013). Thus, ECM nanofibrils or networks can modulate cellular fate or reorganize the tissue architecture or even change the progression of cancer metastasis. For example, the osteochondral interface for bone development undergoes nanofibril gradual transitions by the shifting of cell number, density, polarization, orientation, and nanofibril arrangement along the osteochondral interface (Ren et al., 2016; Jadin et al., 2005; Kronenberg, 2003). In pathological contexts, the ECM nanofibril can undergo remodeling (Martinez-Vidal et al., 2021; Goetz et al., 2011), which is a progressive transition to ECM anisotropy that occurs in many cancers (Martinez-Vidal et al., 2021; Di Martino et al., 2022; Park et al., 2020; Mouw et al., 2014).

Spheroids or tumoroids as multicellular aggregates embedded in an extracellular matrix are a prevalent model to mimic the natural microenvironment. The bottom-up assembly of a spatially ordered aggregate made

✉ Yuan YAO, yyao1@zju.edu.cn
* The two authors contributed equally to this work
Yuan YAO, https://orcid.org/0000-0001-5262-5115

Received Mar. 16, 2023; Revision accepted May 8, 2023;
Crosschecked xxx. xx, 20xx; Published online xxx. xx, 20xx

from multiple cells based on the assembly principle is a highly promising strategy for tissue engineering (Mueller et al., 2020; Rasoulinejad et al., 2020). Over the last decade, artificial materials acting as the extracellular matrix have facilitated multiple-cell aggregation, organization, differentiation, and functionalization (Alegret et al., 2019; Roi et al., 2019; Landry et al., 2018; Malafaya et al., 2007; Grassi et al., 2019; Chen et al., 2017; Hale et al., 2018; Ortega-Prieto et al., 2018; Rossi et al., 2018). Spheroid formation requires multiple-cell assembly based on a scaffold matrix for mechanical support or biochemical signals (Edelman, 1983; Hegedüs et al., 2006). Artificial scaffold matrices for 3D culture systems can be derived from natural compounds to synthetic polymers. For example, decellularized matrix, electrospun nanofiber, hydrogel functionalized with peptides, or polymer-based macroporous scaffolds have been investigated for their varying functions in facilitating spheroid formation (Grassi et al., 2019; Rossi et al., 2018; Roerink et al., 2018; Jaeckel et al., 2018; Sun et al., 2007; Mohan et al., 2014; Louis et al., 2017). The as-formed units usually have a representative microstructure and biological function to their actual tissue counterparts (Tuveson and Clevers, 2019; Gonzalez-Rodriguez et al., 2012; Steinberg, 1962). The artificial extracellular matrix in 3D culture systems, ranging from natural derivatives to synthetic polymers (Grassi et al., 2019; Rossi et al., 2018; Roerink et al., 2018; Jaeckel et al., 2018), provides a spatial scaffold as mechanical support (Rossi et al., 2018; Drost and Clevers, 2018; Amaral and Pasparakis, 2016). However, improving the processing efficiency (assembly time, spheroid dimension) and experimental throughput remain a challenge, as does the fabrication reproducibility, and scale-up capacity of such materials (Lawlor et al., 2021).

Bioengineering tools and diversified nanomaterials modify the aggregating microenvironment for more efficient cell assembly (Cruz et al., 2017; Garreta et al., 2019; Broutier et al., 2017; Bryant et al., 2019; Bagley et al., 2017; Homan et al., 2019; Phipson et al., 2019; Karzbrun et al., 2018; Bergmann et al., 2018; Jager et al., 2018; Miller et al., 2019; Qian et al., 2018). Biocompatible, long, flexible cellulose nanofibrils (CNFs) have been applied as biomaterials in tissue engineering as scaffolds (Ferreira et al., 2020; Yang et al., 2020; Mittal et al., 2018; Zhang et al., 2020; Curvello et al., 2020; Krüger et al., 2020), and have been increasingly popular in preparing functional scaffolds due to being cost-effective and straightforward (Ferreira et al., 2020; Yang et al., 2020; Mittal et al., 2018; Zhang et al., 2020). Nanocellulose-based biomaterials such as foams and aerogels can be synthesized effortlessly using green, scalable approaches (Ferreira et al., 2020; Yang et al., 2020; Mittal et al., 2018; Zhang et al., 2020; Karageorgiou and Kaplan, 2005; Abdul Khalil et al., 2014; Nechyporchuk et al., 2016; Nechyporchuk et al., 2016; Reid et al., 2017; Al-Qararah et al., 2015; Martoïa et al., 2016; Hu et al., 2014). The biocompatibility and physicochemical properties of CNFs make them a promising candidate for biomedical engineering (Curvello et al., 2020; Krüger et al., 2020; Park et al., 2015; Thunberg et al., 2015; Abouzeid et al., 2018). Herein, we developed an effective CNF-driven method to facilitate spheroid formation. The strategy of CNF matrix-driven formation of spheroid (CMDO) involves the use of CNFs as a matrix quantitatively integrated into multiple cells. We validated this method in multiple cell types (including cancer cell lines, fibroblast cells, and hepatocytes). The as-fabricated tumoroid or spheroid represent the replication of the physiological structure of the actual tissue counterpart.

Materials and Methods

CNF preparation

Never-dried sulfite softwood pulp (10 g) with a hemicellulose content of 13.8 wt% and lignin content of 0.7% (Nordic Paper, Sweden) was placed into a three-necked round-bottom flask at a pulp concentration of 1.0 wt%. Subsequently, 156 mg of 2,2,6,6-tetramethylpiperidine-1-oxyl (TEMPO, Sigma-Aldrich) and 1,028 mg of sodium bromide (NaBr, Sigma-Aldrich) were added to the pulp, followed by mixing. Then, 30 mL of NaClO (14% solution, VWR International) was added to the mixture dropwise under stirring. Further oxidization of the pulp was conducted with 1% w/v NaClO2 in acetate buffer at pH 4.8 for 48 h. Following oxidation, the fibers were thoroughly washed with distilled water and disintegrated by passing through a microfluidizer. Finally, a CNF solution with a concentration of ~0.7 wt% and a charge density of 1476 μeq g^{-1} was obtained.

AFM characterization

The surface charge density of CNFs was measured by polyelectrolyte titration at pH 9, with a poly (diallyldimethylammonium chloride) solution (PDADMAC). The topologic structures were assessed using a dimension ICON atomic force microscopy (AFM) fast scanning system (Bruker, Germany) set to tapping mode.

Cell culture

MDA-MB-231, A549, Min6, TTF, and L929 cells were obtained from the Chinese Academy of Sciences (Shanghai, China). A pancreatic cancer cell line was obtained from a xenograft mouse cell. All cell lines were maintained in Dulbecco's Modified Eagle Medium (DMEM) with 10% fetal bovine serum (FBS) and 1X penicillin/streptomycin. Mouse hepatocytes were cultured in previously reported medium (Katsuda et al., 2017). Cell viability was examined by a Cell Counting Kit-8 (Dojindo).

Mass Spectrometry

TMT labeling: freshly prepared cell pellets were lysed using 8 M urea in 100 mM of Tris-HCl at pH 8.5. The protein concentration was measured by the BCA assay (Pierce), wherein 100 μg of each sample was transferred to a new tube for reduction and alkylation with Tris (2-carboxyethyl) phosphine and iodoacetamide, respectively. We took an equal amount of peptide for tandem mass tag (TMT) labeling based on the peptide concentration by following the manufacturer's protocol (Thermo Fisher Scientific, Waltham, MA, USA). The desalted peptide was analyzed using modified MudPIT separation. The sample mixture was analyzed on an Easy-nLC1000 chromatograph (Thermo Scientific).

Quantitative proteomics

Tandem mass spectrometry (MS/MS) analysis was performed by an Orbitrap Elite ETD mass spectrometer (Thermo Scientific) equipped with a nano-electrospray ionization source using distal 2-kV spray voltage. The full-scan resolution was set to 60,000 and MS/MS scan resolution was set to 30,000.

Bioinformatics analysis

Protein identification and quantification were conducted with the Integrated Proteomics Pipeline (IP2, http://integratedproteomics.com/). MS/MS spectra were applied against a Swiss-Prot *Homo sapiens* database using ProLuCID and DTASelect2.0. The differentially expressed lists were subjected to Ingenuity Pathway Analysis (IPA, Qiagen, Ingenuity Systems) and STRING for biological canonical pathways, functions, and network analysis. These analyses were performed herein as proof-of-knowledge to help classify, model, analyze, and understand complex biological and chemical systems.

Dimension measurement of spheroid

Images of CMDOs were captured by a Motic stereoscope (BM2000, 4X) with six replicates for each sample and processed by CellProfiler (https://cellprofiler.org/) using a customized pipeline. The measurement unit of MaximumRadius was the size of the **spheroid**.

Quantitative polymerase chain reaction (qPCR)

The total RNA of target cells was isolated with Trizol Reagent (Life/Invitrogen), and qPCR was performed with SYBR® Premix Ex Taq™ II with ROX (Takara) on a StepOnePlus™ PCR System (ThermoFisher Scientific). The primer sequences are listed in Table 1.

Table 1. Primer sequences for *qPCR.*

Gene	Primers
Afp-F	CTTCCCTCATCCTCCTGCTAC
Afp-R	ACAAACTGGGTAAAGGTGATGG
Alb-F	TGCTTTTTCCAGGGGTGTGTT

Alb-R	TTACTTCCTGCACTAATTTGGCA
Hnf4α-F	CACGCGGAGGTCAAGCTAC
Hnf4α-R	CCCAGAGATGGGAGAGGTGAT
Cyp3a11-F	TGGTCAAACGCCTCTCCTTGCTG
Cyp3a11-R	ACTGGGCCAAAATCCCGCCG
Krt19-F	GGGGGTTCAGTACGCATTGG
Krt19-R	GAGGACGAGGTCACGAAGC
Tbx3-F	GAGGCCAAGGAACTTTGGGA
Tbx3-R	AGGGAACATTCGCCTTCCTG
Sox9-F	TGCTGGTGTGGTGAAAGGTT
Sox9-R	CCAGGAGCAACAAAGTTGGC
β-Actin-F	GGCTGTATTCCCCTCCATCG
β-Actin-R	CCAGTTGGTAACAATGCCATGT

Histology and immunohistochemistry

All samples were fixed in 4% paraformaldehyde by standard protocols. The fixed samples were stained with hematoxylin and eosin (H&E) for histopathological evaluation, and the images were processed with Leica THUNDER Imager (Leica, Germany).

Statistical analysis

Statistical differences were assessed using an unpaired Student's t-test by GraphPad Prism software. The significance levels were set at $*p<0.05$, $**p<0.01$, and $***p<0.001$, whereas $p>0.05$ was considered as not significant.

Results and Discussion

CNF matrix-driven formation of spheroids (CMDO)

In the CMDO system, CNFs (Fig. S1) were prepared as the biomimetic extracellular matrix. They were fabricated by following a previous report (Kobayashi et al., 2014), which yielded individual nanofibrils with a coniferous shape of 20–30 nm in width and 300-500 nm in length (Fig. 1). The properties of these CNFs are suitable for spheroid formation. CNFs are low-cost and biocompatible, with good performance on cell viability (Ferreira et al., 2020; Yang et al., 2020; Mittal et al., 2018; Zhang et al., 2020). The length/width dimension of as-fabricated CNFs is similar to the size of natural collagen nanofibrils (Holmes et al., 2018; Robins et al., 2006; Winkler et al., 2001; Fang et al., 2013; Davies, 2013), allowing the construction of a biomimetic microenvironment. In living tissues, cells exist in complex microenvironments, with cells in a 3D niche and interacting with the extracellular matrix. Hence, the flexible CNFs, based on their biomimetic nanostructure, should allow fast multi-cell aggregation for CDMO. The spheroid was achieved within 48 h (Fig. 1), with a significant improvement in processing efficiency compared to cells grown in Matrigel, with the latter taking 1-3 weeks and yielding small cell clusters (Badea et al., 2019; Xiao et al., 2022). Thus, it was confirmed that CNFs are required for spheroid formation because the control group without CNF failed to form a whole unit.

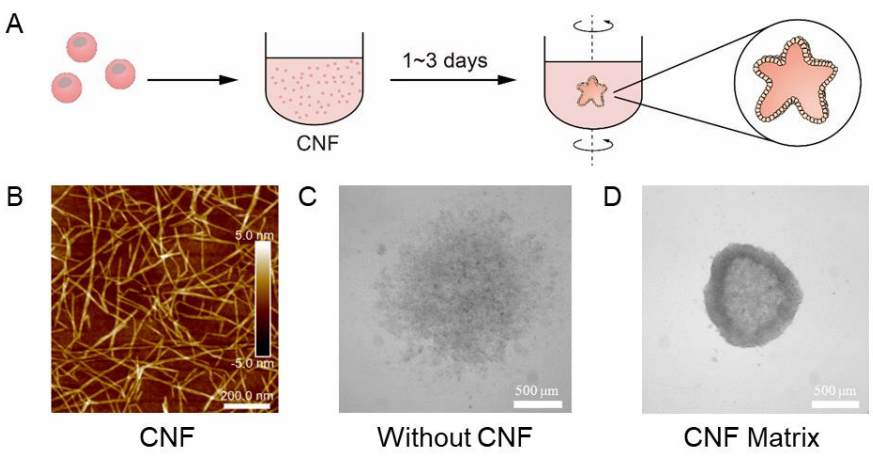

Fig. 1 Cellulose nanofibril (CNF) matrix-driven formation of spheroids (CMDO). (A) The strategy of CMDO. (B) AFM images of CNFs at a gradient concentration of 0.76 wt%. (C) Pancreatic cancer cell aggregate without CNFs (48 h). (D). Pancreatic cancer cell spheroid formation (48 h).

Furthermore, it was observed that the formation of tumoroid was dependent on CNF concentration (Fig. S2). To this end, a concentration of 0.38-0.76 μg/mL of CNFs was the optimal range for the formation of spheroids, to efficiently drive cell assembly into a single, integrated unit (Fig. S2). CNFs at lower concentrations (0-0.12 μg/mL) only formed small clusters sparsely dispersed in culture media (Fig. S2). Thus, by tuning the CNF concentration, the fabrication of CMDOs is controllable: the clustered or dispersed cells are assembled into aggregates with pre-set dimensions. To better understand the formation process, fluorescence images were used to explore the aggregation process for 24 h (Fig. 2A). H&E staining allowed the assessment of microstructure of the formed spheroids (Fig. 2B,C), which showed that spheroids were found in a mesostructured space surrounded by ring-shaped condensate cells (Lawlor et al., 2021; Saito et al., 2019; Fujii et al., 2016).

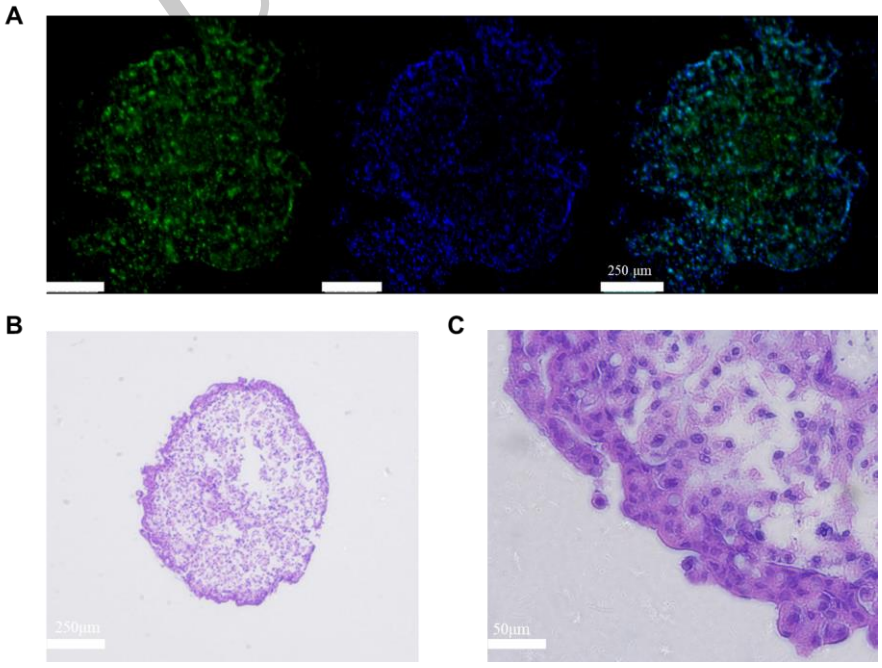

Fig. 2 Microscopic Images of Spheroids. (A) Immunostaining of aggregated spheroids (with 0.38 μg/mL

CNFs) at 24 h: Actin staining (green); DAPI (blue); and merged image. (B, C). H&E staining at 48 h (pancreatic cancer cell spheroids with 0.38 μg/mL CNFs).

Quantitative proteomics for tumoroids

In order to understand the protein-protein interactions during spheroid formation, we conducted quantitative proteomics. Changes in protein expression occurring within the spheroid initiation phase (0-24 h) might be vital in developing this complex tumor-like structure. However, the molecular mechanisms involved in the onset of tumoroid remain elusive. We performed systematic quantitative proteomics involving TMT labeling, which allowed the simultaneous identification and quantification of the protein expression profile.

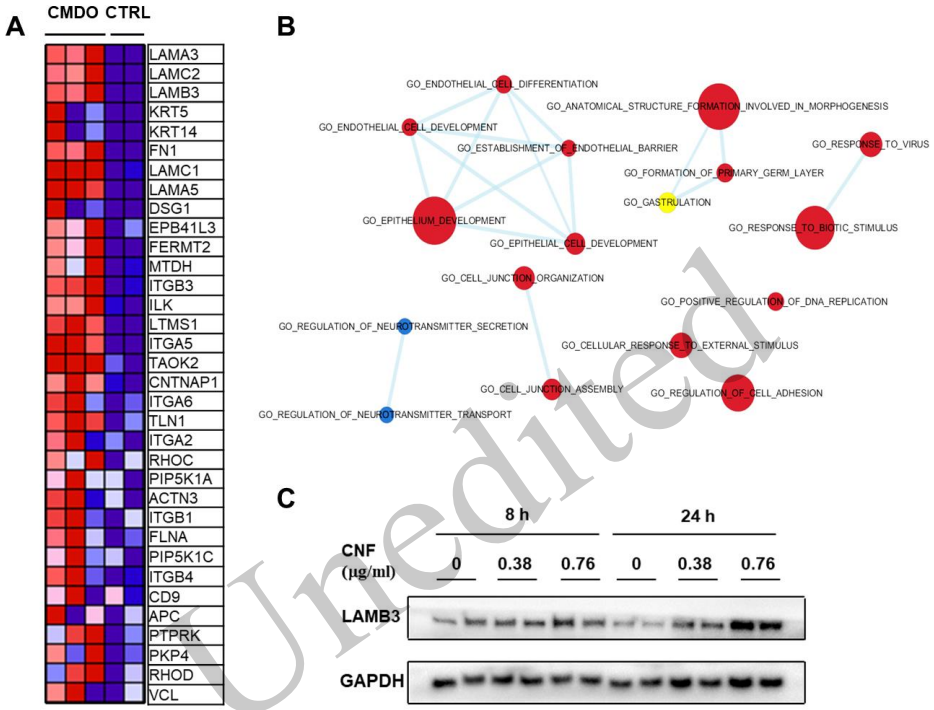

Fig. 3 Quantitative proteomics for tumoroids. (A) Heatmap of proteins related to cell junction and assembly during tumoroid formation (red represents upregulation while blue represents downregulation). (B) IPA protein function clusters based on quantitative proteomics (red represents upregulation while blue represents downregulation). (C) Western blot of LAMB3 at different CNF gradients, with GAPDH acting as control.

The proteomic trajectories implicated in molecular mechanisms relevant to cell death and survival, cellular development, cellular growth, and proliferation were observed at 8 h. The proteomics profile transformed into one of cancer pathogenesis, cellular movement, and tissue development at 24-48 h (Fig. S3). These protein expression changes corresponded with the physiological features of the aggregating process at 8 h (Figure S3) and the stabilized stage at 24-48 h (Fig. S3). Numerous metabolic processes participated in epithelial cell development, cell junction organization, assembly, and related functions. Most of the identified proteins were classified into cell adhesion, movement and communication, which was a response to the microenvironmental change (Fig. 3B). The heatmap (Fig. S3) showed the proteomic profile during aggregation, and two enrichments during epithelial cell development (Fig. S4), cell adhesion and movement (Fig. S5) were also clearly illustrated. The enhancement of laminin (Fig. 3A) indicated cell movement and cell-cell communication, which was in good agreement with the results of IPA analysis (Fig. 3B) and protein–protein networks on STRING (Fig. S6). Laminin is a protein present in the extracellular matrix of organs or tissues, providing support and attachment for cells (Aumailley, 2013). Together with other extracellular matrix proteins, laminin molecules form sheets

and drive the cells to establish connective tissue (Rohn et al., 2018; Nguyen and Senior, 2006; Miner and Yurchenco, 2004). Furthermore, *LAMB3*, encoding the laminin protein, regulates cell movement and attachment (Zhu et al., 2020; Jung et al., 2018; Chung et al., 2014; Fitsialos et al., 2008) and is directly involved in the formation and organization of basement membranes during morphogenesis (Chung et al., 2014; Fitsialos et al., 2008; Buchroithner et al., 2004). Therefore, we validated its expression profile by Western blot (Fig. 3C) and found it to be highly promoted during tumoroid formation.

CDMO generates highly reproducible spheroids

We next assessed the reproducibility of CDMO on 96-well plates. With a given number of initiating cells and dosage of CNFs, the reproducibility of CMDO was high as shown by six repeats for each CNF concentration at 48 h (Fig. 4A). Furthermore, the stabilization of CMDO was achieved within 2 days, indicating significant improvement in processing efficiency compared with control groups without CNF. Additionally, the resulting tumoroid showed morphological homogeneity (Fig. 4A). Cell viability and dimension accuracy were reproducible across all 96 wells (Figs. 4B,4C).

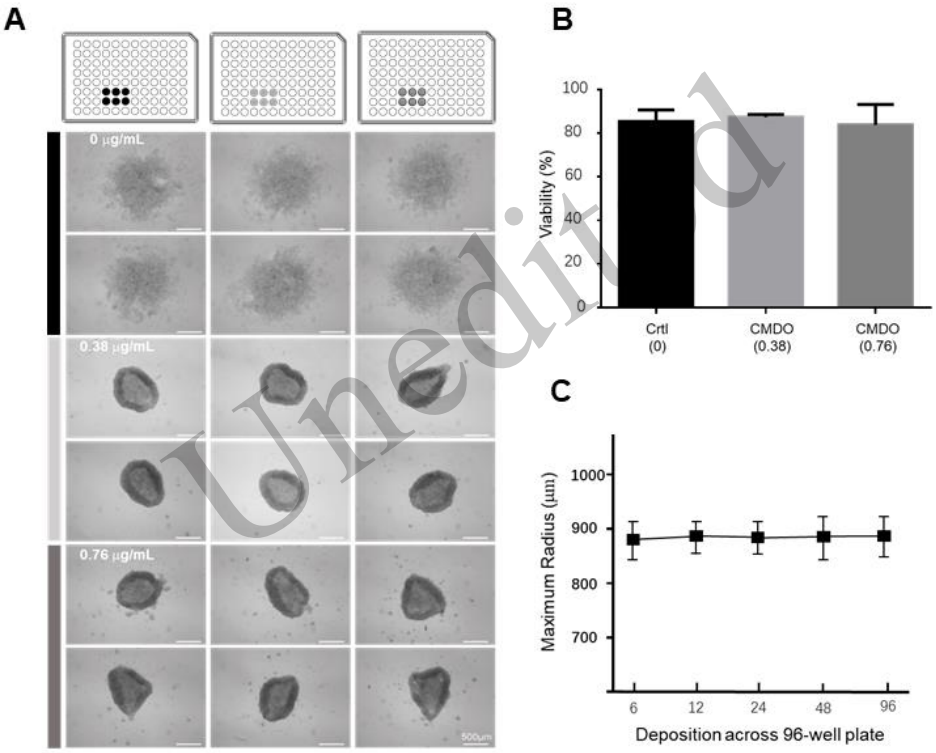

Fig. 4 Experimental reproducibility of CDMO. (A) Experimental reproducibility of pancreatic cancer cell spheroids on 96-well plates. The reproducibility was high, as evidenced by six repeats for each CNF concentration. (B) Viability of tumoroid and PBS group as control. (C) The dimension of spheroids (measured by maximum radius) within the 96-well plate.

Application by CDMO on different cell types

We further evaluated the performance of CMDO using different cell types, including cancer cell lines (A549 and MDA-MB-231), fibroblast cell line (L929), tail-tip fibroblasts (TTF), β-cells (Min6), and mouse hepatocytes (Hmm). A larger number of cells was found to generate greater-sized spheroids (Figs. 5A-F). The experimental reproducibility was high but with a slight standard deviation. Thus, CNFs were regarded as useful as a universal biomimetic scaffold that dynamically facilitates cell aggregation and spheroid formation (Figs. 5B-F). The cell type was detected to determine the shape, conformation and dimension of the as-formed

spheroid. Cancer cells all exhibited a spheroidal morphology, whereas β-cells exhibited a polygonal shape (Fig. 5G). Spheroids grown from L929 cells showed a typical round conformation, while TTF presented a condensation architecture (Fig. 7G).

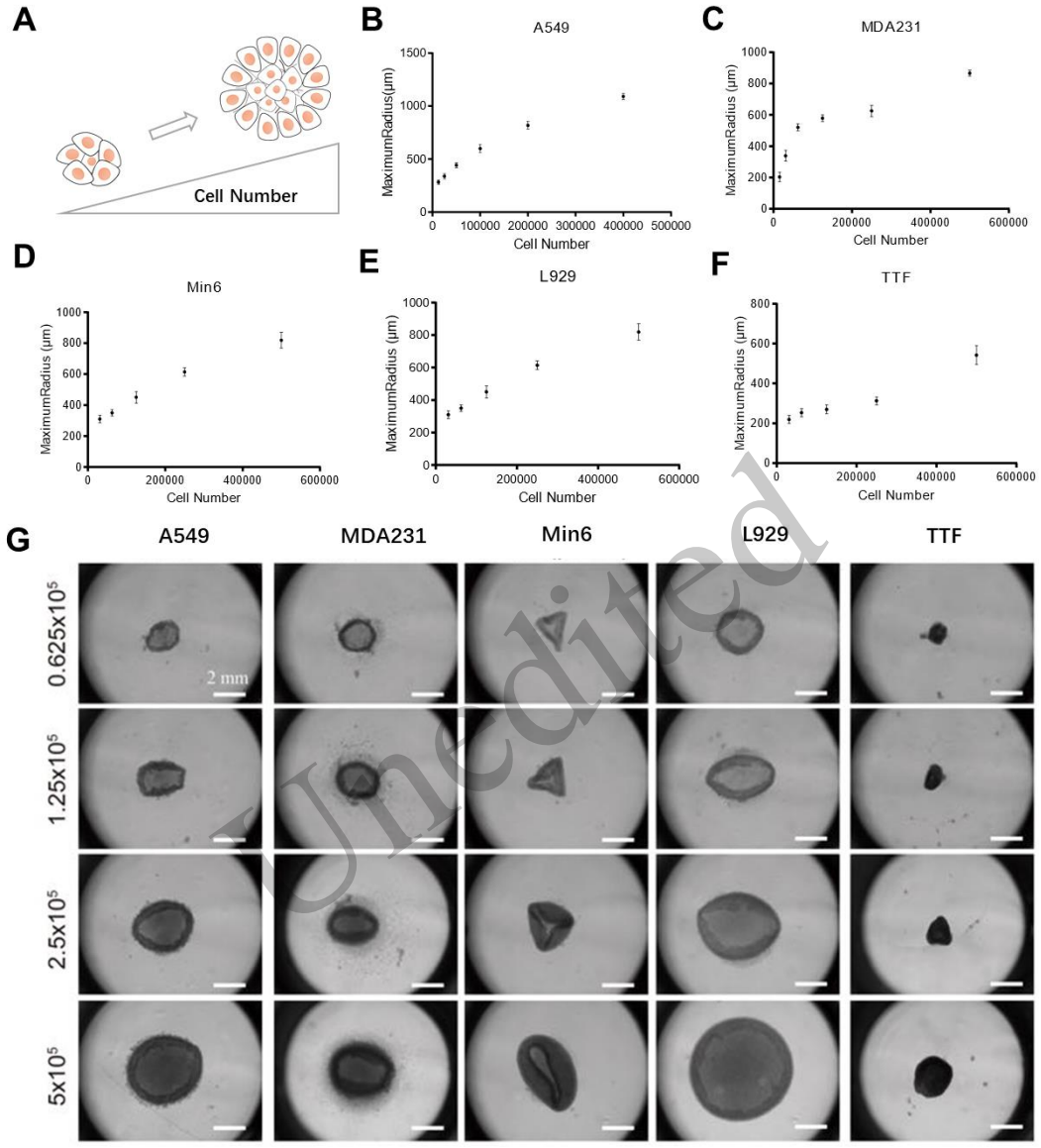

Fig. 5 CNF-induced spheroid formation at 48 h with increasing cell numbers.(A) Illustration of the relationship between spheroid dimension and cell number. Plots of spheroid size versus cell number for (B) A549, (C) MDA-MB-231, (D) Min6, (E) L929, and (F) TTF. (G) Brightfield images of CNF-induced spheroid formation at 48 h with increasing cell numbers (scale bar, 2 mm).

Hepatocyte spheroid by CDMO

Hepatocytes are the main components and functional cells of the liver (Katsuda et al., 2017). Herein, we constructed a hepatocyte spheroid by CMDO. CNFs were able to drive mouse hepatocytes into a spheroid with excellent reproducibility (Fig. S7). An integrated and stable hepatocyte spheroid array with hepatic function is in high demand for clinical research and the pharmaceutical industry. Thus, we built a high-throughput hepatocyte array, wherein liver spheroids were formed in unified and controlled dimensions. For each

hepatocyte spheroid, the hepatic function was validated by functional gene expression (Fig. 6). The expression of functional liver markers was significantly increased (hepatocytes markers: *Alb*, *Hnf4α*, *Cyp3a11*; cholangiocytes markers: *Krt19*), suggesting parallel lineage specification into hepatocytes and polarized cholangiocytes (Fig. 6). Furthermore, the hepatocyte spheroids exhibited higher expression of liver stem cell markers, such as *Afp*, *Tbx3*, and *Sox9*.

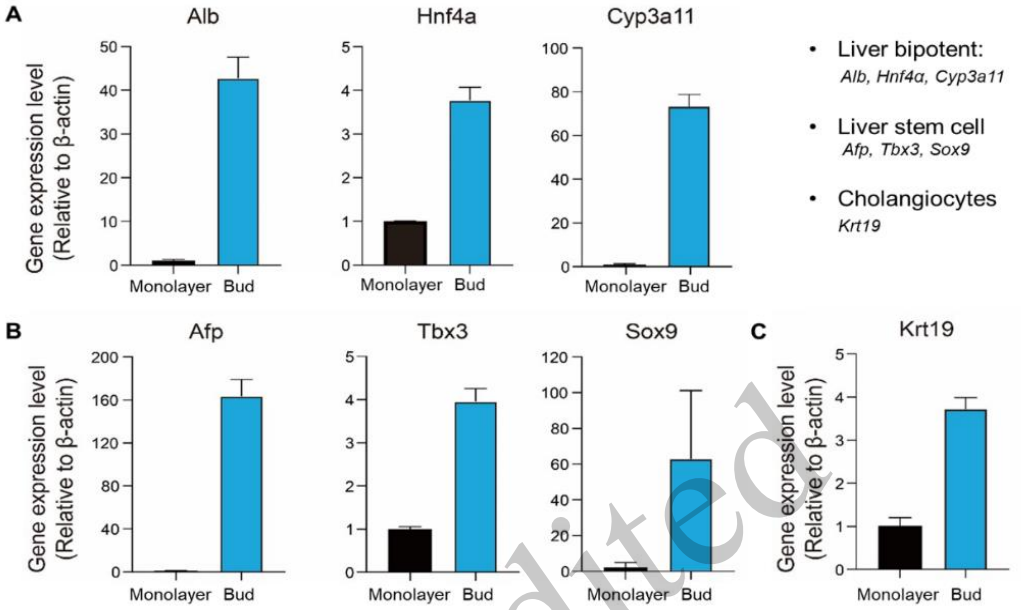

Fig. 6. Comparison of liver function-related gene profiles between monolayer cells and spheroids (monolayer culture is represented by the standard collagen dish coating culture method). (A) Hepatocyte markers: *Alb*, *Hnf4α*, *Cyp3a11*; (B) liver stem cell markers: *Afp*, *Tbx3*, *Sox9*; (C) cholangiocyte markers: *Krt19*.

Conclusion

In this study, we developed a nanofibril-driven technology for multi-cell spheroid formation as a strategy of CDMO. This nanofibril-integrated technology effectively promoted cell aggregation into a well-organized unit that enhanced the physiological structure and biological function. This approach was demonstrated as practical, reproducible, and validated using various cell types. In addition, CNF-based CMDOs were shown to facilitate spatiotemporal support for spheroid or tumoroid formation.

Declaration of competing interest

The authors declare no competing financial interest.

Availability of data and materials

All data generated or analyzed during this study are included in this published article, for further detailed information, please refer to yyao1@zju.edu.cn.

Authorship contribution statement

Yuan Yao performed the following parts of this project: conceptualization, methodology, validation, investigation, writing-original draft, visualization, project administration and funding acquisition. Yi Lu and Guo Li complete the methodology, investigation, data organization and manuscript writing. Guo Li organized the data and manuscript validation and investigation with the assist of Yeqiu Li.

Compliance with ethics guidelines

Compliance with ethics guidelines Yi LU, Guo LI, Yeqiu LI,and Yuan YAO declare that they have no

conflict of interest. This paper does not contain any studies with human subjects performed by any of the authors. Cell lines were obtained from the second affiliated hospital of Nanchang University under the ethic regulation BR/AF/SG-04/1.0.

Acknowledgments

This work was supported by the National Natural Science Foundation of China (nos. 32071347), ZJU-Hangzhou Global Scientific and Technological Innovation Center, Zhejiang University (02020200-K02013008), joint laboratory grant from Jiangsu Wuzhong Aesthetics Biotech Co. Ltd, and the starting grant of ShanghaiTech University. We also would like to thank the iBiofoundary and Core Facility of Institute for Intelligent Bio/Chem Manufacturing, Hangzhou Global Scientific and Technological Innovation Center (China) for fabrication and analysis.

References

Tuveson D, Clevers H, 2019. Cancer modeling meets human organoid technology. Science, 364(6444):952-955. https://doi/10.1126/science.aaw6985

Gonzalez-Rodriguez D, Guevorkian K, Douezan S, et al., 2012. Soft matter models of developing tissues and tumors. Science, 338(6109):910-7. https://doi: 10.1126/science.1226418

Steinberg MS, 1962. On the mechanism of tissue reconstruction by dissociated cells, iii. free energy relations and the reorganization of fused, heteronomic tissue fragments. Proc Natl Acad Sci U S A, 48(10):1769-76. https://doi: 10.1073/pnas.48.10.1769

Tevis KM, Colson YL, Grinstaff MW, 2017. Embedded Spheroids as Models of the Cancer Microenvironment. Adv Biosyst, 1(10):1700083. https://doi: 10.1002/adbi.20170008

J. Chen, J. Zhang, L. Yang, et al., 2023. Facile suspension culture protocol of the liver biliary organoids, Bio-Design and Manufacturing, 6(1):8.

Ren J, Wang Y, Yao Y, et al., 2019. Biological Material Interfaces as Inspiration for Mechanical and Optical Material Designs. Chem Rev, 119(24):12279-12336. https://doi: 10.1021/acs.chemrev.9b00416

Huang C, Dai J, Zhang XA, 2015. Environmental physical cues determine the lineage specification of mesenchymal stem cells. Biochim Biophys Acta, 1850(6):1261-6. https://doi: 10.1016/j.bbagen.2015.02.011

Yeatts AB, Choquette DT, Fisher JP, 2013. Bioreactors to influence stem cell fate: augmentation of mesenchymal stem cell signaling pathways via dynamic culture systems. Biochim Biophys Acta, 1830(2):2470-80. https://doi: 10.1016/j.bbagen.2012.06.007

Ren X, Wang F, Chen C, et al., 2016. Engineering zonal cartilage through bioprinting collagen type II hydrogel constructs with biomimetic chondrocyte density gradient. BMC Musculoskelet Disord, 17:301. https://doi: 10.1186/s12891-016-1130-8

Jadin KD, Wong BL, Bae WC, et al., 2005. Depth-varying density and organization of chondrocytes in immature and mature bovine articular cartilage assessed by 3d imaging and analysis. J Histochem Cytochem, 53(9):1109-19. https://doi: 10.1369/jhc.4A6511.2005

Kronenberg HM. 2003. Developmental regulation of the growth plate. Nature, 423(6937):332-6. https://doi: 10.1038/nature01657

Martinez-Vidal L, Murdica V, Venegoni C, et al., 2021. Causal contributors to tissue stiffness and clinical relevance in urology. Commun Biol, 4(1):1011. https://doi: 10.1038/s42003-021-02539-7

Goetz JG, Minguet S, Navarro-Lérida I, et al., 2011. Biomechanical remodeling of the microenvironment by stromal caveolin-1 favors tumor invasion and metastasis. Cell, 146(1):148-63. https://doi: 10.1016/j.cell.2011.05.040

Di Martino JS, Nobre AR, Mondal C, et al., 2022. A tumor-derived type III collagen-rich ECM niche regulates tumor cell dormancy. Nat Cancer, 3(1):90-107. https://doi: 10.1038/s43018-021-00291-9

Park D, Wershof E, Boeing S, et al., 2020. Extracellular matrix anisotropy is determined by TFAP2C-dependent regulation of cell collisions. Nat Mater, 19(2):227-238. https://doi: 10.1038/s41563-019-0504-3

Mouw JK, Ou G, Weaver VM, 2014. Extracellular matrix assembly: a multiscale deconstruction. Nat Rev Mol Cell Biol, 15(12):771-85.
https://doi: 10.1038/nrm3902

Mueller M, Rasoulinejad S, Garg S, et al.,2020. The Importance of Cell-Cell Interaction Dynamics in Bottom-Up Tissue Engineering: Concepts of Colloidal Self-Assembly in the Fabrication of Multicellular Architectures. Nano Lett, 20(4):2257-2263.
https://doi: 10.1021/acs.nanolett.9b04160

Rasoulinejad S, Mueller M, Nzigou Mombo B, et al., 2020. Orthogonal Blue and Red Light Controlled Cell-Cell Adhesions Enable Sorting-out in Multicellular Structures. ACS Synth Biol, 9(8):2076-2086
https://doi: 10.1021/acssynbio.0c00150.

Alegret N, Dominguez-Alfaro A, Mecerreyes D, 2019. 3D Scaffolds Based on Conductive Polymers for Biomedical Applications. Biomacromolecules, 20(1):73-89.
https://doi: 10.1021/acs.biomac.8b01382

Roi A, Ardelean LC, Roi CI, et al., 2019. Oral Bone Tissue Engineering: Advanced Biomaterials for Cell Adhesion, Proliferation and Differentiation. Materials, 12(14):2296.
https://doi: 10.3390/ma12142296

Landry MJ, Rollet FG, Kennedy TE, et al., 2018. Layers and Multilayers of Self-Assembled Polymers: Tunable Engineered Extracellular Matrix Coatings for Neural Cell Growth. Langmuir, 34(30):8709-8730.
https://doi: 10.1021/acs.langmuir.7b04108

Malafaya PB, Silva GA, Reis RL, 2007. Natural-origin polymers as carriers and scaffolds for biomolecules and cell delivery in tissue engineering applications. Adv Drug Deliv Rev, 59(4-5):207-33.
https://doi: 10.1016/j.addr.2007.03.012

Grassi L, Alfonsi R, Francescangeli F, et al., 2019. Organoids as a new model for improving regenerative medicine and cancer personalized therapy in renal diseases. Cell Death Dis, 10(3):201.
https://doi: 10.1038/s41419-019-1453-0

Chen YW, Huang SX, de Carvalho ALRT, et al., 2017. A three-dimensional model of human lung development and disease from pluripotent stem cells. Nat Cell Biol, 19(5):542-549. https://doi: 10.1038/ncb3510

Hale LJ, Howden SE, Phipson B, et al., 2018. 3D organoid-derived human glomeruli for personalised podocyte disease modelling and drug screening. Nat Commun, 9(1):5167.
https://doi: 10.1038/s41467-018-07594-z

Ortega-Prieto AM, Skelton JK, Wai SN, et al., 2018. 3D microfluidic liver cultures as a physiological preclinical tool for hepatitis B virus infection. Nat Commun, 9(1):682.
https://doi: 10.1038/s41467-018-02969-8

Rossi G, Manfrin A, Lutolf MP, 2018. Progress and potential in organoid research. Nat Rev Genet, 19(11):671-687.
https://doi: 10.1038/s41576-018-0051-9

Edelman GM, 1983. Cell adhesion molecules. Science, 219(4584):450-7.
https://doi: 10.1126/science.6823544

Hegedüs B, Marga F, Jakab K, et al., 2006. The interplay of cell-cell and cell-matrix interactions in the invasive properties of brain tumors. Biophys J, 91(7):2708-16.
https://doi: 10.1529/biophysj.105.077834

Roerink SF, Sasaki N, Lee-Six H, et al., 2018. Intra-tumour diversification in colorectal cancer at the single-cell level. Nature, 556(7702):457-462.
https://doi: 10.1038/s41586-018-0024-3

Jaeckel S, Kaller M, Jackstadt R, et al., 2018. Ap4 is rate limiting for intestinal tumor formation by controlling the homeostasis of intestinal stem cells. Nat Commun, 9(1):3573.
https://doi: 10.1038/s41467-018-06001-x

Sun T, Norton D, McKean RJ, et al., 2007. Development of a 3D cell culture system for investigating cell interactions with electrospun fibers. Biotechnol Bioeng, 97(5):1318-28. https://doi: 10.1002/bit.21309

Mohan N, Gupta V, Sridharan B, et al., 2014. The potential of encapsulating "raw materials" in 3D osteochondral gradient scaffolds. Biotechnol Bioeng, 111(4):829-41.
https://doi: 10.1002/bit.25145

Louis F, Pannetier P, Souguir Z, et al., 2017. A biomimetic hydrogel functionalized with adipose ECM components as a microenvironment for the 3D culture of human and murine adipocytes. Biotechnol Bioeng, 114(8):1813-1824.
https://doi: 10.1002/bit.26306

Drost J, Clevers H, 2018. Organoids in cancer research. Nat Rev Cancer, 18(7):407-418. https://doi: 10.1038/s41568-018-0007-6

Amaral AJ, Pasparakis G, 2016. Rapid Formation of Cell Aggregates and Spheroids Induced by a "Smart" Boronic Acid

Copolymer. ACS Appl Mater Interfaces, 8(35):22930-41.
https://doi: 10.1021/acsami.6b07911

Lawlor KT, Vanslambrouck JM, Higgins JW, et al., 2021. Cellular extrusion bioprinting improves kidney organoid reproducibility and conformation. Nat Mater, 20(2):260-271. https://doi: 10.1038/s41563-020-00853-9

Cruz NM, Song X, Czerniecki SM, et al., 2017. Organoid cystogenesis reveals a critical role of microenvironment in human polycystic kidney disease. Nat Mater, 16(11):1112-1119. https:// doi: 10.1038/nmat4994

Garreta E, Prado P, Tarantino C, et al., 2019. Fine tuning the extracellular environment accelerates the derivation of kidney organoids from human pluripotent stem cells. Nat Mater, 18(4):397-405.
https://doi: 10.1038/s41563-019-0287-6

Broutier L, Mastrogiovanni G, Verstegen MM, et al., 2017. Human primary liver cancer-derived organoid cultures for disease modeling and drug screening. Nat Med, 23(12):1424-1435.
https://doi: 10.1038/nm.4438

Bryant KL, Stalnecker CA, Zeitouni D, et al., 2019. Combination of ERK and autophagy inhibition as a treatment approach for pancreatic cancer. Nat Med, 25(4):628-640.
https://doi: 10.1038/s41591-019-0368-8

Bagley JA, Reumann D, Bian S, et al., 2017. Fused cerebral organoids model interactions between brain regions. Nat Methods, 14(7):743-751.
https://doi: 10.1038/nmeth.4304

Homan KA, Gupta N, Kroll KT, et al., 2019. Flow-enhanced vascularization and maturation of kidney organoids in vitro. Nat Methods, 16(3):255-262.
https://doi: 10.1038/s41592-019-0325-y

Phipson B, Er PX, Combes AN, et al., 2019. Evaluation of variability in human kidney organoids. Nat Methods, 16(1):79-87.
https://doi: 10.1038/s41592-018-0253-2

Karzbrun E, Kshirsagar A, Cohen SR, et al., 2018. Human Brain Organoids on a Chip Reveal the Physics of Folding. Nat Phys, 14(5):515-522.
https://doi: 10.1038/s41567-018-0046-7

Bergmann S, Lawler SE, Qu Y, et al., 2018. Blood-brain-barrier organoids for investigating the permeability of CNS therapeutics. Nat Protoc, 13(12):2827-2843.
https://doi: 10.1038/s41596-018-0066-x

Jager M, Blokzijl F, Sasselli V, et al., 2018. Measuring mutation accumulation in single human adult stem cells by whole-genome sequencing of organoid cultures. Nat Protoc, 13(1):59-78.
https://doi: 10.1038/nprot.2017.111

Miller AJ, Dye BR, Ferrer-Torres D, et al., 2019. Generation of lung organoids from human pluripotent stem cells in vitro. Nat Protoc, 14(2):518-540.
https://doi: 10.1038/s41596-018-0104-8

Qian X, Jacob F, Song MMet al., 2018. Generation of human brain region-specific organoids using a miniaturized spinning bioreactor. Nat Protoc, 13(3):565-580.
https://doi: 10.1038/nprot.2017.152

Ferreira F V, Otoni C G, France K, et al., 2020. Porous nanocellulose gels and foams: Breakthrough status in the development of scaffolds for tissue engineering. Materials Today, 37, 126-141.
https:// doi: 10.1016/j.mattod.2020.03.003

Yang X, Reid MS, Olsén P, et al., 2020. Eco-Friendly Cellulose Nanofibrils Designed by Nature: Effects from Preserving Native State. ACS Nano, 14(1):724-735.
https://doi: 10.1021/acsnano.9b07659

Mittal N, Ansari F, Gowda V K, et al., 2018. Multiscale Control of Nanocellulose Assembly: Transferring Remarkable Nanoscale Fibril Mechanics to Macroscale Fibers. ACS Nano, 12(7):6378-6388.
https://doi: 10.1021/acsnano.8b01084

Zhang X, Xiong R, Kang S, et al., 2020. Alternating Stacking of Nanocrystals and Nanofibers into Ultrastrong Chiral Biocomposite Laminates. ACS Nano, 14(11):14675-14685. https://doi: 10.1021/acsnano.0c06192

Curvello R, Kerr G, Micati DJ, et al., 2020. Engineered Plant-Based Nanocellulose Hydrogel for Small Intestinal Organoid Growth. Adv Sci, 8(1):2002135.
https://doi: 10.1002/advs.202002135

Krüger M, Oosterhoff LA, van Wolferen ME, et al., 2020. Cellulose Nanofibril Hydrogel Promotes Hepatic Differentiation of Human Liver Organoids. Adv Healthc Mater, 9(6): e1901658.
https://doi: 10.1002/adhm.201901658

Karageorgiou V, Kaplan D, 2005. Porosity of 3D biomaterial scaffolds and osteogenesis. Biomaterials, 26(27):5474-91.

https://doi: 10.1016/j.biomaterials.2005.02.002

Abdul Khalil HP, Davoudpour Y, Islam MN, et al., 2014. Production and modification of nanofibrillated cellulose using various mechanical processes: a review. Carbohydr Polym, 99:649-65
https://doi: 10.1016/j.carbpol.2013.08.069.

Nechyporchuk O, Belgacem M N, Bras J, 2016. Production of cellulose nanofibrils: A review of recent advances. Industrial Crops and Products, 93:2-25.
https://doi: 10.1016/j.indcrop.2016.02.016

Nechyporchuk O, Belgacem MN, Pignon F, 2016. Current Progress in Rheology of Cellulose Nanofibril Suspensions. Biomacromolecules, 17(7):2311-20.
https://doi: 10.1021/acs.biomac.6b00668

Reid MS, Villalobos M, Cranston ED, 2017. Benchmarking Cellulose Nanocrystals: From the Laboratory to Industrial Production. Langmuir, 33(7):1583-1598.
https://doi: 10.1021/acs.langmuir.6b03765

A.M. Al-Qararah, A. Ekman, T. Hjelt, et al., 2015. A unique microstructure of the fiber networks deposited from foam–fiber suspensions, Colloids and Surfaces A: Physicochemical and Engineering Aspects, 544-553.

F. Martoïa, T. Cochereau, P.J.J. Dumont, et al., 2016. Cellulose nanofibril foams: Links between ice-templating conditions, microstructures and mechanical properties. Materials & Design, 104: 376-391.

K. Hu, D.D. Kulkarni, I. Choi, et al., 2014. Graphene-polymer nanocomposites for structural and functional applications. Progress in Polymer Science, 39(11): 1934-1972.

Park M, Lee D, Shin S, et al., 2015. Effect of negatively charged cellulose nanofibers on the dispersion of hydroxyapatite nanoparticles for scaffolds in bone tissue engineering. Colloids Surf B Biointerfaces, 130:222-8.
https://doi: 10.1016/j.colsurfb.2015.04.014

J. Thunberg, T. Kalogeropoulos, V. Kuzmenko, et al., 2015. In situ synthesis of conductive polypyrrole on electrospun cellulose nanofibers: scaffold for neural tissue engineering. Cellulose, 22(3):1459-1467

Abouzeid RE, Khiari R, Beneventi D, et al., 2018. Biomimetic Mineralization of Three-Dimensional Printed Alginate/TEMPO-Oxidized Cellulose Nanofibril Scaffolds for Bone Tissue Engineering. Biomacromolecules, 19(11):4442-4452.
https://doi: 10.1021/acs.biomac.8b01325

Katsuda T, Kawamata M, Hagiwara K, et al., 2017. Conversion of Terminally Committed Hepatocytes to Culturable Bipotent Progenitor Cells with Regenerative Capacity. Cell Stem Cell, 20(1):41-55.
https://doi: 10.1016/j.stem.2016.10.007

Kobayashi Y, Saito T, Isogai A, 2014. Aerogels with 3D ordered nanofiber skeletons of liquid-crystalline nanocellulose derivatives as tough and transparent insulators. Angew Chem Int Ed Engl, 53(39):10394-7.
https://doi: 10.1002/anie.201405123

Holmes DF, Lu Y, Starborg T, et al., 2018. Collagen Fibril Assembly and Function. Curr Top Dev Biol, 130:107-142.
https://doi: 10.1016/bs.ctdb.2018.02.004

S.P. Robins, 2006. CHAPTER 2 - Fibrillogenesis and Maturation of Collagens, in: M.J. Seibel, S.P. Robins, J.P. Bilezikian (Eds.), Dynamics of Bone and Cartilage Metabolism (Second Edition), Academic Press, Burlington, pp. 41-53.

S. Winkler, D.L. Kaplan, 2001. Biosynthesized Materials: Properties and Processing, in: K.H.J. Buschow, R.W. Cahn, M.C. Flemings, B. Ilschner, E.J. Kramer, S. Mahajan, P. Veyssière (Eds.), Encyclopedia of Materials: Science and Technology, Elsevier, Oxford, pp. 609-615.

Fang M, Goldstein EL, Matich EK, et al., 2013. Type I collagen self-assembly: the roles of substrate and concentration. Langmuir, 29(7):2330-8.
https://doi: 10.1021/la3048104

J.A. Davies, 2013. Chapter 3 - The Power and Limitations of Self-Assembly, in: J.A. Davies (Ed.), Mechanisms of Morphogenesis (Second Edition), Academic Press, Boston, pp. 17-30.

Badea MA, Balas M, Hermenean A, et al., 2019. Influence of Matrigel on Single- and Multiple-Spheroid Cultures in Breast Cancer Research. SLAS Discov, 24(5):563-578.
https://doi: 10.1177/2472555219834698

Xiao RR, Jin L, Xie N, et al., 2022. Establishment and large-scale validation of a three-dimensional tumor model on an array chip for anticancer drug evaluation. Front Pharmacol, 13:1032975.
https://doi: 10.3389/fphar.2022.1032975

Saito Y, Muramatsu T, Kanai Y, et al., 2019. Establishment of Patient-Derived Organoids and Drug Screening for Biliary Tract Carcinoma. Cell Rep, 27(4):1265-1276.e4.
https://doi: 10.1016/j.celrep.2019.03.088

Fujii M, Shimokawa M, Date S, et al., 2016. A Colorectal Tumor Organoid Library Demonstrates Progressive Loss of Niche

Factor Requirements during Tumorigenesis. Cell Stem Cell, 18(6):827-838.
https://doi: 10.1016/j.stem.2016.04.003

Aumailley M. 2013. The laminin family. Cell Adh Migr, 7(1):48-55.
https://doi: 10.4161/cam.22826

Rohn F, Kordes C, Castoldi M, et al., 2018. Laminin-521 promotes quiescence in isolated stellate cells from rat liver. Biomaterials, 180:36-51.
https://doi: 10.1016/j.biomaterials.2018.07.008

Nguyen NM, Senior RM, 2006. Laminin isoforms and lung development: all isoforms are not equal. Dev Biol, 294(2):271-9.
https://doi: 10.1016/j.ydbio.2006.03.032

Miner JH, Yurchenco PD, 2004. Laminin functions in tissue morphogenesis. Annu Rev Cell Dev Biol, 20:255-84.
https://doi: 10.1146/annurev.cellbio.20.010403.094555

Zhu Z, Song J, Guo Y, et al., 2020. LAMB3 promotes tumour progression through the AKT-FOXO3/4 axis and is transcriptionally regulated by the BRD2/acetylated ELK4 complex in colorectal cancer. Oncogene, 39(24):4666-4680.
https://doi: 10.1038/s41388-020-1321-5

Jung SN, Lim HS, Liu L, et al., 2018. LAMB3 mediates metastatic tumor behavior in papillary thyroid cancer by regulating c-MET/Akt signals. Sci Rep, 8(1):2718.
https://doi: 10.1038/s41598-018-21216-0

Chung H, Jung H, Lee JH, et al., 2014. Keratinocyte-derived laminin-332 protein promotes melanin synthesis via regulation of tyrosine uptake. J Biol Chem, 289(31):21751-9. https://doi: 10.1074/jbc.M113.541177

Fitsialos G, Bourget I, Augier S, et al., 2008. HIF1 transcription factor regulates laminin-332 expression and keratinocyte migration. J Cell Sci, 121(Pt 18):2992-3001.
https://doi: 10.1242/jcs.029256

Buchroithner B, Klausegger A, Ebschner U, et al., 2004. Analysis of the LAMB3 gene in a junctional epidermolysis bullosa patient reveals exonic splicing and allele-specific nonsense-mediated mRNA decay. Lab Invest, 84(10):1279-88.
https://doi: 10.1038/labinvest.3700164